Tuning the Catalase Activity of Dinuclear Manganese Complexes by Utilizing Different Substituted Tripodal Ligands

Nicole Reddig,[a] Daniel Pursche,[a] Michael Kloskowski,[a] Caroline Slinn,[a] Sascha M. Baldeau,[a] and Annette Rompel*[a]

Keywords: Manganese / Tripodal ligands / Bioinorganic chemistry / Enzyme models

A series of five new dinuclear manganese(II/II) compounds with derivatives of 2-{[bis(pyridin-2-ylmethyl)amino]-methyl}phenol (HL_1) were synthesized and structurally characterized. All complexes crystallize in monoclinic space groups and exhibit Mn···Mn separations in the range of 3.392(8)–3.493(2) Å caused by bis(μ-phenoxo) bridging modes. The derivatives of HL_1 contain either electron-donating or -withdrawing substituents. A correlation between the electronic character of the different ring substituents, the redox potentials of the dinuclear transition metal complexes and the catalase activity has been revealed. In analogy to manganese catalase, all complexes show saturation kinetics at high substrate concentration. The investigated catalase activity places the compounds in the upper range of functional catalase mimics.

Introduction

The manganese catalases are the most intensively studied dinuclear manganese enzymes. By disproportionating hydrogen peroxide into water and dioxygen, manganese catalases protect cells from deleterious effects caused by this harmful by-product of respiration. In addition to heme-type catalases,[1] there is another class of manganese catalases that has been found in three bacterial organisms, *Lactobacillus plantarium*,[2,3] *Thermus thermophilus*,[4,5] and *Thermoleophilum album*.[6] The manganese catalase from *Thermus thermophilus* is the best characterized one. During the catalytic cycle the oxidation states of the dinuclear manganese center change between Mn_2(II/II) and Mn_2(III/III). There are also two inactive forms [Mn_2(II/III) and Mn_2(III/IV)], which are caused by one-electron transitions during the disproportionation of hydrogen peroxide.[7,8]

So far only three functional model systems for the catalase reaction have been described which employ Mn_2(II/II) and Mn_2(III/III) in their catalytic cycles. The first system, $[Mn_2(L^1)(\mu\text{-OAc})]^{2+}$, is based on a heptadentate ligand L^1 [*N*,*N*,*N*′,*N*′-tetrakis(2-methylenebenzimidazolyl)-1,3-diaminopropan-2-ol] and was the first functional catalase mimic.[9–12] The second model system is the [Mn_2(2-OHsalpn)$_2$] [2-OHsalpn = 1,3-bis(salicylideneamino)-2-propanol] system. It has been fully crystallographically and spectroscopically characterized in four different oxidation states and serves as both a structural and functional manganese catalase mimic.[13–15] At the moment the most efficient catalase mimic is based on the ligand bpia [bis(picolyl)-(*N*-methylimidazol-2-yl)amine], which belongs to the class of tripodal ligands. The [Mn_2(bpia)$_2$] system consists of four dinuclear complexes, that mimic structural, spectroscopic and functional features of manganese catalases. $[Mn_2(bpia)_2(\mu\text{-OAc})_2](ClO_4)_2$ and $[Mn_2(bpia)_2(\mu\text{-O})_2](ClO_4)_2$-$(PF_6)\cdot 2CH_3CN$ are the most efficient catalysts using the Mn_2(II/II) and Mn_2(III/IV) redox couple reported to date for the disproportion of hydrogen peroxide.[16]

In this paper we report the synthesis, characterization and catalase activity of five new dinuclear Mn_2(II/II) complexes. They are based on tripodal ligands featuring an N_3O donor set, where the parent ligand is 2-({bis[(pyridin-2-yl)-methyl]amino}methyl)phenol. The phenol moiety of the ligands leads to a bis(μ-phenoxo) bridging motif, leaving one vacant coordination site at each manganese center. These are occupied by two mutually *trans*-positioned chloride ions. The catalytic activity regarding the disproportionation of hydrogen peroxide depends on the ring substituents. It will be shown that electron-withdrawing groups decrease the ability to disproportionate hydrogen peroxide, whereas electron-donating groups increase this ability. The catalase activities of the model compounds described in this paper range between those of [Mn_2(bpia)$_2$] and [Mn_2(2-OHsalpn)$_2$] and place the five dinuclear manganese(II/II) complexes in second position for functional manganese catalase mimics.

Results and Discussion

Reaction of manganese(II) chloride tetrahydrate with the corresponding ligand under basic conditions yields the di-

[a] Institut für Anorganische und Analytische Chemie, Westfälische Wilhelms-Universität,
Wilhelm-Klemm-Str. 8, 48149 Münster, Germany
Fax: (internat.) + 49-251/833-8366
E-mail: rompela@uni-muenster.de

nuclear manganese complexes $[Mn_2(L_1)_2Cl_2]\cdot 2CH_2Cl_2$ (**1**), $[Mn_2(L_2)_2Cl_2]\cdot C_2H_5OH$ (**2**), $[Mn_2(L_3)_2Cl_2]\cdot 2CH_2Cl_2$ (**3**), $[Mn(L_4)_2Cl_2]\cdot 2CH_2Cl_2$ (**4**) and $[Mn_2(L_5)_2Cl_2]$ (**5**). All compounds crystallize in the monoclinic crystal system. Complexes **1**−**3** crystallize in the space group $P2_1/c$ (no.14), while **4** and **5** crystallize in $I2/a$ (no.15). Each unit cell consists of four complex molecules, except for compound **3**, where only two complex molecules can be found. Either eight (**1**), four (**2**, **3**, and **4**), or no (**5**) solvent molecules complete the unit cells. The manganese ions are in the oxidation state +II. They are bis(μ-phenoxo)-bridged by the ligands' phenol groups resulting in Mn···Mn-distances in the range from 3.392(8) Å (**5**) to 3.493(2) Å (**4**). The distorted octahedral coordination environment of each manganese center is formed by an N_3O_2Cl donor set, where, except for the chloride ions, all donor atoms are provided by the ligands. The crystal structure of the metal complexes are depicted below. Selected bonds and angles for all complexes are listed in Table 1.

Table 1. Selected distances [Å] and angles [°] of **1**−**5**

	1[a]	**2**[a]	**3**	**4**	**5**
Mn(1)···Mn(1a)[b]	3.411(1)	3.440(1)	3.406(2)	3.493(2)	3.392(8)
Mn(1)−Cl(1)	2.451(2)	2.426(1)	2.472(3)	2.425(9)	2.454(1)
Mn(1)−O(1)	2.119(4)	2.138(2)	2.147(3)	2.156(2)	2.138(2)
Mn(1)−O(1a)[b]	2.203(4)	2.199(2)	2.173(3)	2.205(2)	2.142(2)
Mn(1)−N(1)	2.367(5)	2.360(3)	2.330(4)	2.305(2)	2.372(2)
Mn(1)−N(2)	2.348(5)	2.263(3)	2.399(4)	2.313(2)	2.273(2)
Mn(1)−N(3)	2.254(5)	2.288(3)	2.338(4)	2.361(2)	2.312(2)
Mn(1)−O(1)−Mn(1a)[b]	105.2(2)	105.0(9)	104.1(1)	106.4(7)	104.8(7)
Cl(1)−Mn(1)−O(1)	111.2(1)	111.6(7)	117.5(1)	118.6(6)	114.7(5)
Cl(1)−Mn(1)−O(1a)[b]	105.2(1)	101.5(7)	97.0(1)	101.3(5)	101.5(6)
Cl(1)−Mn(1)−N(1)	155.7(1)	157.1(7)	154.9(1)	154.2(6)	152.9(7)
Cl(1)−Mn(1)−N(2)	88.1(1)	98.2(9)	96.3(1)	89.1(7)	93.2(6)
Cl(1)−Mn(1)−N(3)	96.0(1)	90.5(8)	90.6(2)	96.6(6)	88.5(8)
O(1)−Mn(1)−O(1a)[b]	76.0(1)	75.0(9)	75.9(1)	73.6(7)	75.2(7)
O(1)−Mn(1)−N(1)	85.4(2)	84.4(9)	85.0(1)	84.9(6)	84.4(7)
O(1)−Mn(1)−N(2)	92.9(2)	146.9(1)	88.5(1)	147.4(7)	150.6(8)
O(1)−Mn(1)−N(3)	151.1(2)	92.2(1)	148.5(2)	86.8(7)	87.8(7)
O(1a)−Mn(1)−N(1)[b]	95.8(2)	98.4(9)	99.5(1)	95.3(6)	102.0(8)
O(1a)−Mn(1)−N(2)[b]	165.0(2)	85.5(1)	163.0(1)	85.0(7)	90.8(7)
O(1a)−Mn(1)−N(3)[b]	87.9(2)	165.0(1)	87.4(2)	158.1(6)	162.6(7)
N(1)−Mn(1)−N(2)	73.0(2)	72.1(1)	71.9(1)	72.8(7)	73.2(8)
N(1)−Mn(1)−N(3)	72.3(2)	72.1(1)	71.4(2)	72.9(7)	72.5(9)
N(2)−Mn(1)−N(3)	97.8(2)	101.9(1)	103.1(2)	108.0(7)	102.9(8)

[a] Bond lengths and angles for Mn(2) are omitted for clarity. [b] Mn(1a) = Mn(2) and O(1a) = O(2) for **1**.

$[Mn_2(L_1)_2(Cl)_2]\cdot 2CH_2Cl_2$ (1; Figure 1): Mononuclear Cu,[17] Fe,[18] Re,[19] and Zn[20] complexes of HL_1 are known. In addition, dinuclear Fe,[21,22] Cu,[23] and Zn[20] complexes have also been published.

The Mn−N bond lengths around Mn(1) range from 2.254(5) for Mn(1)−N(3) to 2.367(5) Å for Mn(1)−N(1). The distances for the Mn(1)−O bonds are 2.119(4) [O(1)] and 2.203(4) Å [O(2)]. The longest bond to be found is Mn(1)−Cl(1) [2.451(2) Å]. Except for small deviations, the manganese−donor atom bonds for Mn(2) are in the same range as for Mn(1). The average N(1)−Mn(1)−N(X) (X = 2, 3) and N(4)−Mn(2)−N(Y) (Y = 5, 6) angles of 72.7 and 72.3° differ significantly from 90° and show the distortion from octahedral geometry due to constraints imposed by the ligand.

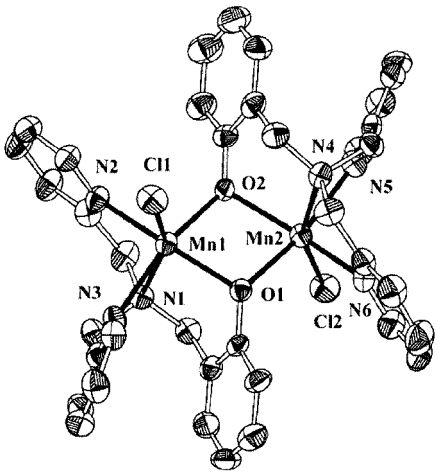

Figure 1. Ellipsoid plot of **1** showing 50% probability thermal ellipsoids; hydrogen atoms are omitted for clarity

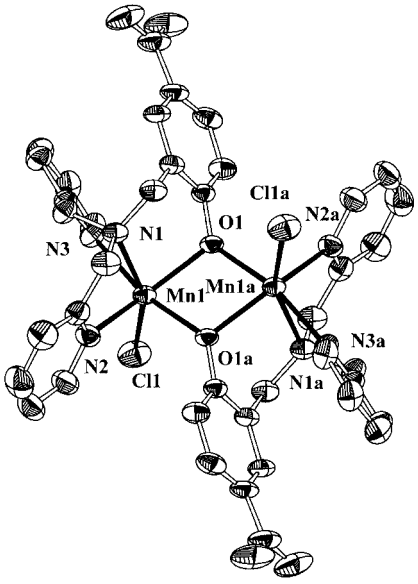

Figure 2. Ellipsoid plot of **2** showing 50% probability thermal ellipsoids; hydrogen atoms are omitted for clarity

$[Mn_2(L_2)_2(Cl)_2]\cdot C_2H_5OH$ (2; Figure 2): In 1987 an analogous structure of complex **2** was published by Nishida with NCS ligands instead of chloride ligands ($P2_1/n$).[24] In addition, mono- and dinuclear copper complexes[23,25−27] and mononuclear iron complexes[18,28] of HL_2 have been described in the literature.

There are two half complex molecules and one ethanol molecule in the asymmetric unit. Both manganese(II) centers of each independent complex molecule are related by a crystallographic inversion center. The coordination environment of Mn(1) is described as it is representative of both Mn(1) and Mn(2). The longest bond to be found is

Mn(1)−Cl(1) [2.426(1) Å]. The chloride ion is bonded *trans* to the aliphatic nitrogen atom N(1), with a bond length of 2.360(3) Å. This is considerably longer than the manganese−pyridine distances Mn(1)−N(2) [2.263(3) Å] and Mn(1)−N(3) [2.288(3) Å]. The average distance for the Mn−O bonds is 2.168 Å.

The five-membered chelate rings containing Mn(1), N(1), N(2/3) cause a distortion from an ideal octahedral geometry. Hence, for the average N(1)−Mn(1)−N(X) (X = 2, 3) angles a deviation of 17.8° from the ideal 90° angle is observed. The distortion is shown best in the angles including *trans*-bonded donor atoms. The largest difference from linearity occurs in the angles O(1)−Mn(1)−N(2) [146.9(1)°].

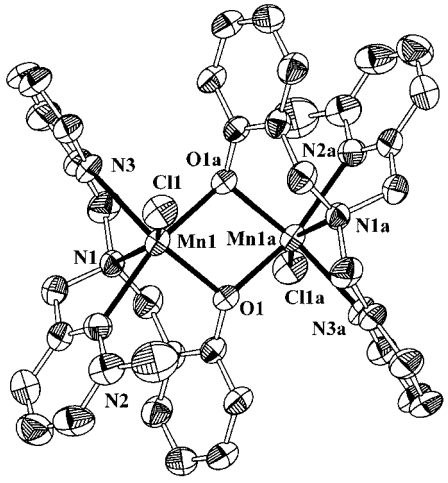

Figure 3. Ellipsoid plot of **3** showing 50% probability thermal ellipsoids; hydrogen atoms and a depiction of the chloride disorder are omitted for clarity

$[Mn_2(L_3)_2(Cl)_2]\cdot 2\ CH_2Cl_2$ (3; Figure 3): There is a crystallographic inversion center found in the middle of the dinuclear complex, rendering the two halves of the molecule crystallographically equivalent. The chloride ion is disordered. The occupation factors for both forms were refined to 0.71 and 0.29. The manganese−chlorine bonds show an average value of 2.407 Å. The aliphatic nitrogen atom N(1) is bonded *trans* to the chloride ion, with a bond length of 2.330(4) Å. This is shorter than the manganese−pyridine distances. The bond Mn(1)−N(2) [2.399(4) Å] is the longest manganese−nitrogen bond in the complex, which can be attributed to the steric effects of the methyl substituent in the *ortho* position of N(2). The Mn−O bond lengths are in the same range. The average N(1)−Mn(1)−N(X) (X = 2, 3) angle of 71.7° differs significantly from 90° and shows the distortion from octahedral geometry due to constraints imposed by the ligand.

$[Mn_2(L_4)_2(Cl)_2]\cdot 2CH_2Cl_2$ (4; Figure 4) and $[Mn_2(L_5)_2(Cl)_2]$ (5; Figure 4): A crystallographic inversion center in the middle of the complexes generates the corresponding symmetric equivalent half. Mn(1) is surrounded by an N_3O_2Cl donor set while the position of the chloride ion is slightly disordered. The occupation factors for both

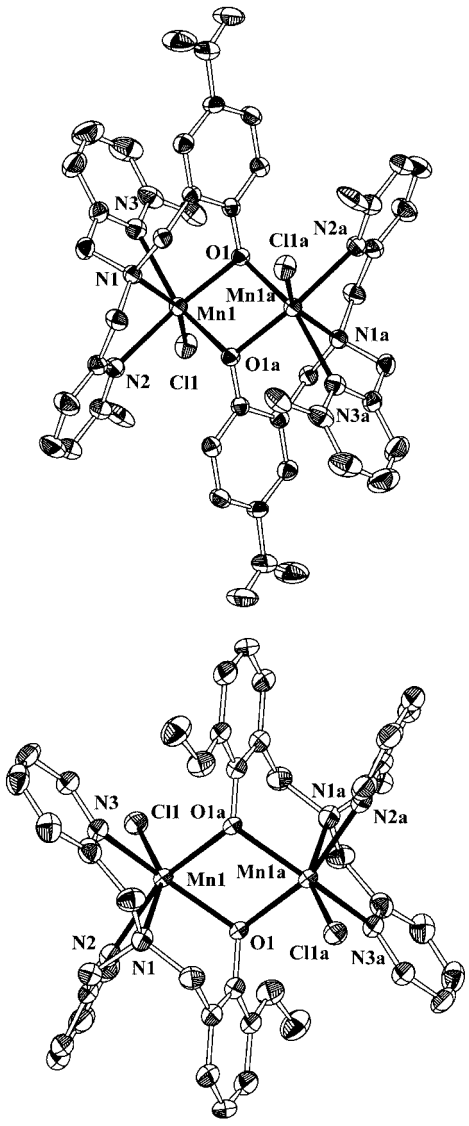

Figure 4. Ellipsoid plots of **4** (top) and **5** (bottom) showing 50% probability thermal ellipsoids; hydrogen atoms and a depiction of the chloride disorder are omitted for clarity

positions have been refined to 0.84 and 0.16 for complex **4** and 0.95 and 0.05 for **5**. In addition, compound **4** shows a disorder of the methyl substituent, where the occupation factors for both positions have been refined to 0.80 and 0.20.

The Mn(1)−Cl(1) bonds are the longest to be found in both compounds and show values of 2.425(9) Å (**4**) and 2.454(1) Å (**5**). The aliphatic nitrogen atom N(1) is bonded *trans* to the chloride ion with distances for **4** of 2.305(2) Å and for **5** of 2.372(2) Å to Mn(1). As expected, in **5** both pyridine nitrogen atoms N(2) and N(3) exhibit shorter bonds to the metal center with values of 2.273(2) Å and 2.312(2) Å, respectively. In complex **4** the Mn(1)−N(2, 3) distances are longer compared to Mn(1)−N(1) (see Table 1). This can be attributed to the steric effects of the disordered methyl substituent in the *ortho* position of N(2) and N(3), respectively. The two oxygen atoms O(1) and O(1a)

are bonded *trans* to the aromatic nitrogen atoms N(2) and N(3). Distances of 2.156(2) Å (**4**) and 2.138(2) Å (**5**) for Mn(1)−O(1) and 2.205(2) Å (**4**) and 2.142(2) Å (**5**) for Mn(1)−O(1a) have been determined. The bis(μ-phenoxo)-bridging mode results in Mn···Mn separations of 3.493(2) Å for compound **4** and 3.392(8) Å for complex **5**. The distortion from ideal octahedral symmetry is best clarified by comparing the values for the two angles N(1)−Mn(1)−N(X) (X = 2, 3) and O(1)−Mn(1)−N(2) with their ideal values. The latter differs significantly from the ideal 180° with angles of 147.4(7)° (**4**) and 150.6(8)° (**5**), while the average angles for N(1)−Mn(1)−N(X) (X = 2, 3) deviate by around 17.2° from the ideal 90°.

There is a correlation between the Mn···Mn distances and the type of ring substituent. In particular, the influence of the electron-withdrawing effect of the NO_2 groups, that are *p*-bonded to the phenol oxygen atom in **2** and **4**, is conspicuous. Because of its −M effect the electron density of the phenolic oxygen atom is reduced through the aromatic π-system. This results in a weaker Mn−O bond, leading to larger Mn···Mn distances than in complexes **1**, **3**, and **5**. On the other hand electron-donating groups like methyl and methoxy moieties stabilize the Mn−O bonds resulting in shorter Mn···Mn separations than in the parent complex **1**.

Electrochemistry

The redox potentials of complexes **1**−**5** are summarized in Table 2. Figure 5 shows the cyclic voltammogram of compound **2** in acetonitrile as the most representative.

Table 2. Redox potentials of complexes **1**−**5**

Complex	$E_{1/2}$ (ΔE) [V] vs. Ag/AgCl $Mn_2^{II/II}/Mn_2^{II/III}$
1	0.44 (0.14)
2	0.76 (0.15)
3	0.45 (0.07)
4	0.64 (0.07)
5	0.45 (0.16)

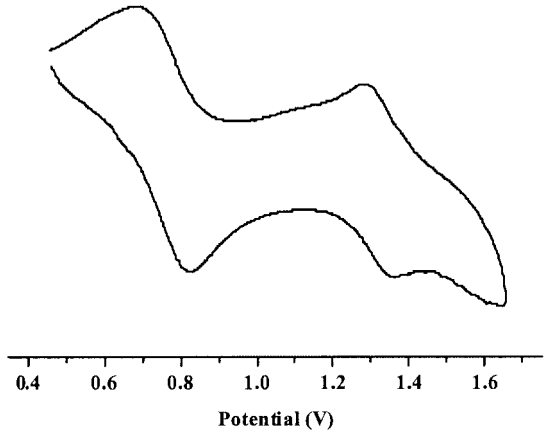

Figure 5. Cyclic voltammogram of **2** in acetonitrile

The observed redox potentials for the oxidation $Mn^{II}Mn^{II}/Mn^{II}Mn^{III}$ are in good agreement with data reported in the literature for similar dinuclear manganese compounds.[29−32]

For a reversible single-electron redox transition an ideal peak separation of 59 mV has to be detected. For compounds **3** and **4** the differences in peak potentials for the first redox transition show little difference from the ideal 59 mV (ΔE = 70 mV). This shift can be attributed to solvent effects.[33] Therefore these waves can clearly be attributed to a single-electron transfer in both complexes from Mn^{II}/Mn^{II} to Mn^{II}/Mn^{III}.

In the case of quasi-reversible electron transitions the determination of *n*, the number of electrons involved in the redox process, is more complicated. The large peak-separation for the first redox transition in the cyclic voltammogram of compounds **1**, **2**, and **5** (ΔE = 140−160 mV) indicates that the electron transfer is slow. For a system undergoing slow electron transfers it has been shown that the number of electrons can be determined using the following equation:[31,34] $\alpha n = 0.048/(|E_p - E_{p/2}|)$.

In the present case a value of 0.5 can be considered for the charge-transfer coefficient α due to the symmetrical shape of the corresponding wave. E_p is the peak potential of the considered wave and $E_{p/2}$ represents the potential value at half the intensity of the peak current. From the obtained data listed in Table 3 one can ascertain that $n = 1$ for the first redox transition.

Table 3. Potential peak values for the $Mn^{II}Mn^{II}/Mn^{II}Mn^{III}$ oxidation in **1**, **2**, and **5**

Compound	E_{pa} [V]	$E_{pa/2}$ [V]	E_{pc}	ΔE [V]
1	0.37	0.46	0.51	0.14
2	0.68	0.78	0.83	0.15
5	0.37	0.48	0.53	0.16

Thus, on the time scale of cyclic voltammetry (250 mV s^{-1}) our investigations lead to the following conclusion. For compounds **1**−**5** the first redox transition can clearly be attributed to a single-electron transfer from $Mn^{II}Mn^{II}$ to $Mn^{II}Mn^{III}$.

It is noteworthy that both oxidation waves in the cyclic voltammogram of **2** differ in intensity by a factor of 1.3. For the remaining complexes this difference is significantly smaller. To further investigate this second oxidation peak, additional electrochemical studies were performed on the pure ligand. In analogy to data reported by Blondin et al., oxidation of the phenolic part of the ligands occurs at higher potentials.[31] Those irreversible, ill-defined cyclic voltammetric traces overlay any supposed oxidation from $Mn^{II}Mn^{III}$ to $Mn^{III}Mn^{III}$.

However, there is a clear correlation between the revealed redox potentials and the type of ring substituent. As shown in Table 2, the increase of the redox potentials for the first transition is directly commensurate with the intensity of the

electron-withdrawing effect of the ring substituents. This was observed before by Walton et al.[35] Their investigations on transition metal redox behavior were based on a series of mononuclear manganese compounds. Using different phenol-substituted triimine and triamine ligands an analogous influence on the redox potential was observed for CH_3O, CH_3, and NO_2 groups as *para*-substituents of the phenol group.

Catalase Activity

Compounds **1**−**5** are stable under ambient conditions and are not oxidized by atmospheric oxygen. All complexes are able to disproportionate hydrogen peroxide in aqueous solution. Like $[Mn(bpia)(\mu\text{-}OAc)]_2(ClO_4)_2$, they are examples of synthetic catalysts showing saturating kinetics at high substrate concentrations (see Figure 6).[16]

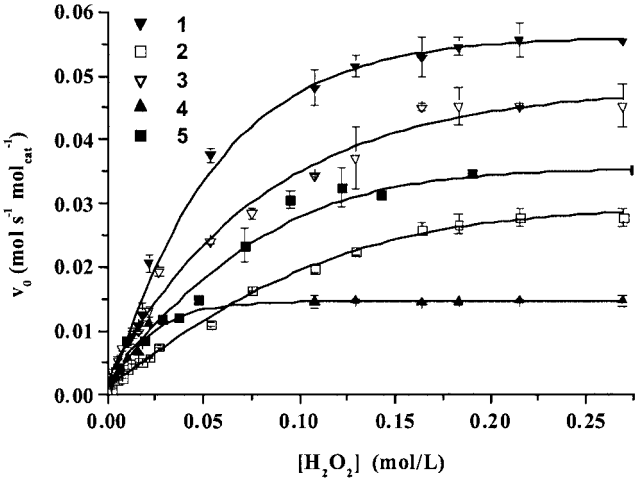

Figure 6. Initial rate of substrate consumption versus substrate concentration at constant concentration of **1**−**5**

Consequently, the data were fitted to the Michaelis−Menten equation, and the *turnover* number k_{cat}, the Michaelis constant K_M and k_{cat}/K_M were determined from the double reciprocal Lineweaver−Burk plot (Figure 7). The values of k_{cat}, K_M and k_{cat}/K_M are listed in Table 4.

Taking K_M as a measure of substrate affinity, the methoxy-substituted compound **5** exhibits the highest affinity for hydrogen peroxide (lowest value of K_M) while the parent complex **1** shows the lowest value for substrate binding (highest value of K_M). This is noteworthy if one considers that the unsubstituted ligand should allow easier access to the metal center, resulting in a higher affinity for hydrogen peroxide. Therefore electronic reasons must be the rate-determining effects for substrate binding. It is conceivable that the methoxy lone pairs interact with the substrate leading to higher substrate binding.

The *turnover number* k_{cat} can be interpreted as the rate of substrate conversion into the corresponding products. Once H_2O_2 is bonded to the metal center the rate of conversion is best for the parent complex **1**, followed by complex **3**

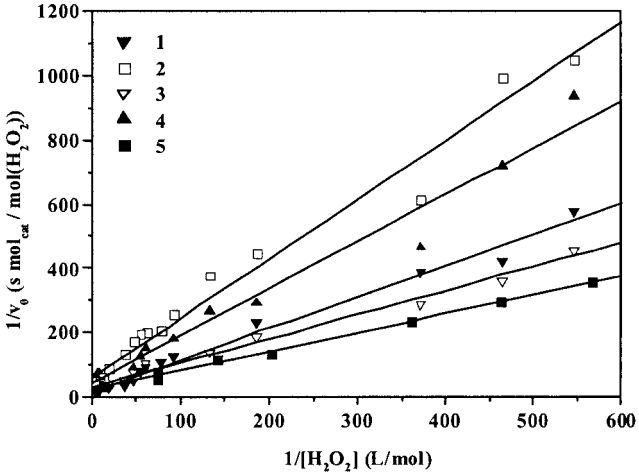

Figure 7. Lineweaver−Burk plots for **1**−**5**

(methyl substituted) and compound **5** (methoxy residue). The slowest complex in terms of *turnovers* is the *p*-nitro-substituted complex **2**, exhibiting a threefold slower catalytic conversion than **1**. The electron-withdrawing effect of the nitro group is presumably the decisive difference. This effect causes a reduction of the electron density of the manganese centers via the aromatic π-system. Since the disproportionation of hydrogen peroxide is a redox process this effect decreases the speed of substrate conversion.

In order to understand the observed kinetic data a comparison of k_{cat}/K_M as a criterion for catalytic efficiency and the determined redox potentials is necessary. By comparing the k_{cat}/K_M criteria of the five complexes a dependence of the rate of the hydrogen peroxide disproportionation on the ring substituents is also observed. Starting with complex **1**, which contains the unsubstituted parent ligand, the activity increases if electron-donating groups like methyl or methoxy substituents are bound to the pyridine or phenol arm (**2** and **5**). Although the methoxy group is bigger than the methyl group, complex **5** is more efficient than **2**. This can be attributed to the increased ability to donate electrons into the aromatic π-system compared to the methyl group. It seems to be that the complexes' catalase activity is more dependent on electronic than on steric effects. Therefore, by using a methoxy substituent k_{cat}/K_M of **5** is larger than for both **1** and **2**. On the other hand k_{cat}/K_M decreases if an NO_2 group is bonded in the *para* position to the bridging phenol oxygen atom. This is caused by its strong electron-withdrawing effect, which reduces the electron density of the manganese centers via the aromatic π-system. The use of both an electron-withdrawing and -donating group, as in **4**, leads to a higher k_{cat}/K_M than for **2**.

As shown by CV experiments (vide supra) the redox potentials correlate with the insertion of electron-withdrawing or -donating substituents. The cyclic voltammograms of compounds **1**, **3** and **5** exhibit lower values for the observed redox transitions, while the corresponding $E_{1/2}$ values for the remaining complexes are shifted to higher potentials. This coherence between the redox potentials and the utilized ring substituents underlines the determined catalase ac-

Table 4. Catalytic activity of manganese catalase and synthetic catalase mimics

	k_{cat} [s^{-1}]	K_M [mM]	k_{cat}/K_M [$M^{-1}\cdot s^{-1}$]	Ref.
Thermus thermophilus catalase	2.6×10^5	83	3.1×10^6	[36]
Lactobacillus plantarum catalase	2.0×10^5	350	0.6×10^6	[7]
Thermoleophilum album catalase	2.6×10^4	15	1.7×10^6	[6]
$[Mn_2(bpia)_2(\mu\text{-}OAc)_2](ClO_4)_2$	1070	31.5	34000	[16]
5	140	18	7800	this work
3	165	24.2	6800	this work
1	283	54.3	5400	this work
4	115.6	33.2	3500	this work
2	87.7	31.8	2750	this work
$[Mn_2(salpn)_2O_2]$	2500	250	1000	[37,38]
$[Mn_2(2\text{-}OHsalpn)_2]$	4.2−21.9	10.2−118.0	160−990	[13,14]
$[Mn_2(tacn)(bipy)(\mu\text{-}O)_2(\mu\text{-}OAc)(MeOH)](ClO_4)_2\cdot MeOH$	13.2[a]	–	–	[39] [b]
$[Mn_2(bpia)_2(\mu\text{-}O)_2](ClO_4)_2(PF_6)\cdot 2CH_3CN$	8.1[a]	–	–	[16]
$[Mn_2(tacn)(\mu\text{-}O)_2(\mu\text{-}OAc)(OAc)_2]$	5.5[a]	–	–	[17] [b]
$[Mn_2(L^1)(\mu\text{-}OAc)(H_2)]^{2+}$	2.1[a]	0.3	700	[9−12] [c]
$[Mn_2(salpentO)(\mu\text{-}OAc)(\mu\text{-}OMe)(MeOH)_2]$	0.66	36	18	[40]
$[Mn(H_2O)_6](ClO_4)_2$	0.0063[a]	–	–	[13]

[a] No saturation kinetics observed/reported. [b] tacn = 1,4,7-trimethyl-1,4,7-triazacyclononane; bpy = 2,2′-bipyridine. [c] L^1 = *N*,*N*,*N*′,*N*′-tetrakis(2-methylenebenzimidazolyl)-1,3-diaminopropan-2-ol.

tivity. This is in good agreement with experiments reported previously concerning the binding efficiency of hydrogen peroxide to the manganese center,[13] where it has been reported that the manganese compounds donating the most electrons have the highest affinity for the substrate.

Since complexes **1**−**5** are hexacoordinate in the solid state it is most likely that at least one chloride ligand is replaced in solution by a solvent molecule that can easily be replaced by the substrate. This has been proved by MALDI experiments (see Exp. Sect.). This soft ionization method ensures that each species in solution is detected without further conversion into fragments. As is shown in the Exp. Sect. either an $[M^+ - Cl]$ or $[M^+ - HCl]$ species was detected in every spectrum. This is convincing evidence that the dinuclear structure is preserved in solution without the coordination of one chloride ion to the dinuclear metal core. Therefore one manganese ion provides a labile coordination site. This is sufficient to disproportionate H_2O_2 as it is postulated for the catalytic cycle of Mn catalase.[7]

The observed catalase activities place the complexes **1**−**5** within approximately three orders of magnitude of the three characterized manganese catalases in terms of both k_2 and k_2/K_M criteria.

Conclusion

The synthesis and structural characterization of five dinuclear manganese(II/II) compounds has been reported. The utilized tripodal ligands share two pyridine and one phenol moiety but differ in the type of substituents coordinated to the aromatic rings. It seems that the electronic character of the different ring substituents tunes the catalase activity, which correlates with the observed redox potentials of the dinuclear transition metal complexes. Groups donating electrons into the aromatic π-system lead to higher catalytic activity involving lower $E_{1/2}$ values while electron-withdrawing substituents cause the opposite effect, namely higher $E_{1/2}$ values and lower catalase activity. All compounds belong to the class of synthetic model complexes showing saturation kinetics at high substrate concentrations. The observed catalase activity places the complexes **1**−**5** within approximately three orders of magnitude of the three characterized manganese catalases in terms of both k_2 and k_2/K_M criteria. Compared to the two most efficient systems $[Mn_2(bpia)_2]$ and $[Mn_2(2\text{-}OHsalpn)_2]$, described by Triller et al.[16] and Gelasco et al.,[13] respectively, compounds **1**−**5** are the second best functional manganese catalase mimics.

Experimental Section

Physical Measurements: IR spectra were recorded with a Perkin−Elmer Spectrum GX FT-IR spectrometer in the range of 4000−400 cm^{-1}. Samples were prepared as KBr pellets. Elemental analyses were carried out with a Perkin−Elmer 2400 Series 2 analyzer. MALDI experiments were performed with a Bruker Daltonics MALDI Reflex IV spectrometer. The compounds were dissolved in the same solvent system as used for the kinetic measurements. Cyclic voltammetric experiments were performed with a BAS CV-27 voltammograph equipped with a BAS C-1B cell stand and a BAS RXY recorder. The concentration of the samples was 1×10^{-3} M in acetonitrile for **2**, 1×10^{-3} M in acetonitrile/DMF (15:1) for **4** and **5**, 3×10^{-3} M in acetonitrile/DMF (15:1) for **1** and **3**. Prior to use, solvents were purified by standard literature methods.[41] Tetrabutylammonium hexafluorophosphate (recrystallized from ethanol) was used as supporting electrolyte at a concentration of 0.1 M. A three-electrode array consisting of a glassy carbon working electrode, a platinum wire counter electrode and an Ag/AgCl reference electrode was used.

Kinetic Measurements: Catalase activities of all complexes were measured at 25 °C on the basis of fluorescence quenching using an oxygen sensor.[42] Hydrogen peroxide solution in water was placed in a vessel equipped with a thermostat (5 mL, prepared in different

concentrations from 36.6% hydrogen peroxide solution in water, concentration determined iodometrically and manganometrically). Before each measurement, a calibration of the oxygen sensor was carried out by saturating the solution with dioxygen (100% dioxygen) and then with argon (0% dioxygen). The dioxygen concentration in dioxygen-saturated water has been determined to be 1.388 mM.[43] After a baseline had been established, 0.1 mL of a 0.01 M solution of the complex in degassed methanol was added, and the oxygen evolution was monitored. The average initial rate over three independent measurements, expressed as $mol(H_2O_2)\cdot s^{-1}\cdot[mol(catalyst)]^{-1}$,[12] was determined by linear regression from the slope of concentration versus time plots.

Syntheses: The ligands HL_3 and HL_4 were prepared according to the previously reported syntheses of HL_1 [21] and HL_2,[44] respectively, using *N*-[(6-methylpyridin-2-yl)methyl]-*N*-(pyridin-2-ylmethyl)amine instead of *N*,*N*-bis(pyridin-2-ylmethyl)amine.

2-[{[(6-Methylpyridin-2-yl)methyl](pyridin-2-ylmethyl)amino}-methyl]phenol (HL_3): Yield: 5.43 g (17 mmol, 75%). $C_{20}H_{21}N_3O$ (319.0): calcd. C 75.24, H 6.58, N 13.17; found C 75.13, H 6.34, N 13.15. ^{1}H NMR (300 MHz, $CDCl_3$): δ = 2.59 (s, 3 H, CH_3), 3.80 (s, 2 H, CH_2), 3.85 (s, 2 H, CH_2), 3.88 (s, 2 H, CH_2), 6.77−7.64 (m, 10 H, Ar-H), 8.57 (d, *J* = 4.8 Hz, 1 H, Ar-H) ppm. ^{13}C NMR (75 MHz, $CDCl_3$): δ = 24.2, 56.9, 59.2, 59.3, 116.6, 118.9, 120.1, 121.7, 122.2, 122.9, 123.3, 129.0, 130.2, 136.7, 137.0, 149.0, 157.6, 157.7, 158.0, 158.5 ppm. IR (KBr): $\tilde{\nu}$ = 3440 cm^{-1} (m, br), 3049 (s), 2956 (s), 2922 (s), 2855 (s), 2801 (s), 2708 (m), 2608 (m), 2256 (w), 2007 (w), 1979 (w), 1935 (w), 1905 (w), 1876 (w), 1789 (w), 1688 (w), 1612 (m), 1583 (vs), 1512 (w), 1488 (vs), 1465 (s), 1437 (s), 1428 (s), 1375 (s), 1362 (s), 1316 (w), 1289 (m), 1246 (w), 1204 (m), 1181 (w), 1161 (m), 1141 (m), 1122 (m), 1091 (m), 1039 (m), 1003 (m), 990 (w), 973 (m), 955 (w), 937 (w), 899 (w), 892 (w), 870 (w), 789 (s), 760 (vs), 717 (m), 646 (w), 604 (m), 558 (m), 542 (w), 479 (m), 444 (m).

2-[{[(6-Methylpyridin-2-yl)methyl](pyridin-2-ylmethyl)amino}-methyl]-4-nitrophenol (HL_4): Yield: 2.4 g (17 mmol, 57%). $C_{20}H_{20}N_4O_3$ (365.1): calcd. C 65.74, H 5.48, N 15.34; found C 65.60, H 5.39, N 15.26. ^{1}H NMR (300 MHz, $CDCl_3$): δ = 2.60 (s, 3 H, CH_3), 3.85 (s, 2 H, CH_2), 3.90 (s, 2 H, CH_2), 3.92 (s, 2 H, CH_2), 6.95−8.12 (m, 9 H, Ar-H), 8.58 (d, *J* = 4.8 Hz, 1 H, Ar-H) ppm. ^{13}C NMR (75 MHz, $CDCl_3$): δ = 24.0, 56.0, 58.8, 59.0, 117.2, 120.0, 122.0, 122.4, 123.2, 123.6, 125.6, 126.6, 137.0, 137.2, 137.9, 148.8, 156.8, 157.9, 161.2, 162.6 ppm. IR (KBr): $\tilde{\nu}$ = 3434 cm^{-1} (m, br), 3074 (m), 3049 (m), 3002 (m), 2930 (m), 2820 (m), 2717 (m), 2491 (w), 1736 (w), 1619 (m), 1600 (m), 1582 (s), 1511 (s), 1488 (s), 1460 (m), 1431 (m), 1377 (m), 1333 (vs), 1292 (s), 1262 (m), 1240 (s), 1178 (m), 1149 (m), 1133 (m), 1110 (m), 1088 (m), 1049 (m), 1009 (m), 976 (m), 931 (w), 904 (w), 878 (m), 839 (m), 823 (m), 750 (s), 733 (m), 641 (w), 610 (w), 566 (w), 511 (w), 494 (w), 450 (m).

The ligand 2-{[bis(pyridin-2-ylmethyl)amino]methyl}-6-methoxyphenol (HL_5) was synthesized as follows.

2-Methoxy-6-{[(pyridin-2-ylmethyl)amino]methyl}phenol: Equivalent amounts of 2-pyridylmethylamine (2.70 g, 25 mmol) and 2-hydroxy-3-methoxybenzaldehyde (3.80 g, 25 mmol) were dissolved in 100 mL of methanol and stirred for 2 h. After reduction with $NaBH_4$ (0.47 g, 12.5 mmol), the solution was stirred for a further 12 h. The mixture was acidified with hydrochloric acid to pH = 1 and, after concentrating under vacuum, extracted with chloroform (5 × 20 mL) to separate side products and impurities. In order to neutralize the hydrochloride, the pH was adjusted to 8 with an aqueous solution of NaOH and the free amine was extracted with chloroform (5 × 20 mL). The combined organic layers were dried ($MgSO_4$) and the solvent was removed under vacuum yielding the oily product. Yield: 5.73 g (23.6 mmol, 94%). ^{1}H NMR (300 MHz, $CDCl_3$): δ = 3.88 (s, 3 H, O-CH_3), 3.92 (s, 2 H, CH_2), 4.02 (s, 2 H, CH_2), 6.59−7.69 (m, 6 H, Ar-H), 8.56 (d, *J* = 4.8 Hz, 1 H, Ar-H).

2-{[Bis(pyridin-2-ylmethyl)amino]methyl}-6-methoxyphenol (HL_5): 2-Methoxy-6-{[(pyridin-2-ylmethyl)amino]methyl}phenol (4.88 g, 20.0 mmol) and 2-chloromethylpyridine hydrochloride (3.28 g, 20.0 mmol) were dissolved in 100 mL of methanol. A pH value of 9 was adjusted by adding solid potassium carbonate. The mixture was stirred at room temperature for 3 d while the pH value was controlled every 24 h. After the remaining K_2CO_3 was filtered off, the mixture was acidified carefully with hydrochloric acid to pH = 1. Further purification was performed with the method described above to yield an orange brown product. Yield: 3.99 g (11.9 mol, 50%). $C_{20}H_{21}N_3O_2$ (335.4): calcd. C 71.62, H 6.31, N 12.53; found C 71.50, H 6.19, N 12.76. ^{1}H NMR (300 MHz, $CDCl_3$): δ = 3.73 (s, 3 H, OCH_3), 3.89 (s, 2 H, CH_2), 3.90 (s, 4 H, CH_2), 6.71 (dd, *J* = 7.6 Hz, *J* = 7.9 Hz, 1 H, Ar-H), 6.74 (d, *J* = 7.9 Hz, 1 H, Ar-H), 6.83 (d, *J* = 7.6 Hz, 1 H, Ar-H), 7.13−7.66 (m, 6 H, Ar-H), 8.57 (d, *J* = 4.8 Hz, 2 H, Ar-H) ppm. ^{13}C NMR (75 MHz, $CDCl_3$): δ = 55.9, 56.7, 59.0, 111.3, 118.5, 122.3, 122.4, 123.2, 123.3, 134.9, 137.0, 146.9, 148.7, 158.2 ppm. IR (KBr): $\tilde{\nu}$ = 3434 cm^{-1} (m, br), 3054 (m), 3010 (m), 2935 (m), 2917 (m), 2835 (m), 2805 (m), 2750 (w), 2609 (w), 1947 (w), 1888 (w), 1586 (s), 1570 (m), 1486 (s), 1472 (s), 1433 (s), 1389 (m), 1372 (m), 1299 (m), 1250 (s), 1235 (s), 1160 (m), 1134 (m), 1073 (s), 1049 (m), 1006 (m), 994 (m), 976 (m), 954 (m), 933 (m), 886 (w), 837 (m), 777 (s), 761 (m), 737 (m), 631 (m), 617 (w), 561 (w), 539 (w), 510 (w), 483 (w), 467 (w).

Synthesis of the Dinuclear Complexes 1−5: All complexes were prepared according to the same method. Equivalent amounts of manganese(II) chloride tetrahydrate (0.25 mmol, 49.5 mg) and corresponding ligand were dissolved in 10 mL of ethanol and triethylamine (0.3 mmol, 42 μL) was added. After stirring the mixture for 12 h, the resulting precipitate was isolated and redissolved in 10 mL of dichloromethane. Crystals suitable for X-ray diffraction analysis were obtained by layering with hexane.

$[Mn_2(L_1)_2(Cl)_2]\cdot 2CH_2Cl_2$ (1): Yield:113.78 mg (0.12 mmol, 47%). $C_{38}H_{36}Cl_2Mn_2N_6O_2$ (789.52): calcd. C 57.81, H 4.60, N 10.64; found C 56.96, H 4.46, N 10.49. MS (MALDI): *m*/*z* = 754 [M^+ − Cl]. IR (KBr): $\tilde{\nu}$ = 3436 cm^{-1} (m, br), 3050 (m), 3021 (m), 3002 (m), 2982 (w), 2954 (m), 2913 (m), 2878 (m), 2830 (m), 2776 (w), 2604 (w), 2497 (w), 1885 (w), 1602 (vs), 1571 (s), 1476 (vs), 1452 (vs), 1396 (w), 1368 (w), 1349 (s), 1326 (w), 1308 (w), 1269 (vs), 1190 (w), 1150 (m), 1129 (m), 1095 (m), 1052 (m), 1037 (m), 1014 (m), 999 (m), 978 (m), 960 (m), 926 (m), 881 (s), 837 (m), 759 (vs), 737 (s), 660 (w), 638 (m), 576 (m), 517 (w), 493 (w), 477 (m).

$[Mn_2(L_2)_2(Cl)_2]\cdot EtOH$ (2): Yield: 155.41 mg (0.17 mmol, 67%). $C_{38}H_{34}Cl_2Mn_2N_8O_6$ (879.51): calcd. C 51.89, H 3.90, N 12.74; found C 51.46, H 3.86, N 12.24. MS (MALDI): *m*/*z* = 843 [M^+ − HCl]. IR (KBr): $\tilde{\nu}$ = 3427 cm^{-1} (s, br), 3056 (w), 2956 (w), 2848 (w), 1719 (m, br), 1600 (s), 1573 (m), 1477 (s), 1437 (m), 1395 (w), 1329 (w), 1286 (vs), 1180 (m), 1153 (m), 1126 (m), 1090 (s), 1051 (m), 1014 (m), 977 (w), 961 (w), 933 (m), 894 (w), 838 (w), 763 (m), 737 (s), 671 (m), 648 (s), 516 (w), 461 (m, br).

$[Mn_2(L_3)_2(Cl)_2]\cdot CH_2Cl_2$ (3): Yield: 106.27 mg (0.12 mmol, 47%). $C_{40}H_{40}Cl_2Mn_2N_6O_2$ (817.58): calcd. C 58.76, H 4.93, N 10.27; found C 58.40, H 4.23, N 9.67. MS (MALDI): *m*/*z* = 780 [M^+ − HCl]. IR (KBr): $\tilde{\nu}$ = 3399 cm^{-1} (s, br), 3054 (m), 3024 (m), 3001 (m), 2963 (m), 2923 (m), 2833 (m), 1907 (w), 1677 (s), 1602 (vs),

Table 5. Details of structure determination, refinement and experimental parameters of compounds **1**−**5**

	1	**2**	**3**	**4**	**5**
Empirical formula	$C_{40}H_{40}Cl_6Mn_2N_6O_2$	$C_{40}H_{40}Cl_2Mn_2N_8O_7$	$C_{41}H_{42}Cl_4Mn_2N_6O_2$	$C_{41}H_{40}Cl_4Mn_2N_8O_6$	$C_{40}H_{42}Cl_2Mn_2N_6O_4$
Formula mass [g/mol]	959.36	925.58	902.33	992.33	851.56
Temperature [K]	213(2)	213(2)	213(2)	100(2)	100(2)
Wavelength [Å]	0.71073	0.71073	0.71073	0.71073	1.54178
Crystal system	monoclinic	monoclinic	monoclinic	monoclinic	monoclinic
Space group	$P2_1/c$ (No. 14)	$P2_1/c$ (No. 14)	$P2_1/n$ (No. 14)	$I2/a$ (No. 15)	$I2/a$ (No. 15)
a [Å]	11.104(2)	20.214(4)	11.870(2)	22.997(5)	21.8425(5)
b [Å]	15.394(3)	11.620(2)	13.171(3)	8.762(2)	8.7350(2)
c [Å]	25.306(5)	17.324(3)	15.417(3)	23.602(5)	21.9876(7)
β [°]	92.80(3)	96.94(3)	111.72(3)	101.37(3)	113.81(1)
V [Å^3]	4320.4(15)	4039.4(13)	2239.2(8)	4662.5(18)	3838.2(1)
Z	4	4	2	4	4
Density (calcd.) [g/cm^3]	1.475	1.522	1.459	1.526	1.470
μ [mm^{-1}]	0.998	0.818	0.965	0.941	7.040
Crystal size [mm]	0.31 × 0.20 × 0.12	0.48 × 0.40 × 0.24	0.40 × 0.40 × 0.32	0.13 × 0.11 × 0.09	0.12 × 0.10 × 0.08
θ range [°]	8.5 ≤ 2θ ≤ 52.0	8.8 ≤ 2θ ≤ 52.0	9.1 ≤ 2θ ≤ 52.0	3.52 ≤ 2θ ≤ 56.58	8.80 ≤ 2θ ≤ 142.36
Index ranges	−13 ≤ h ≤ 13	−24 ≤ h ≤ 24	−14 ≤ h ≤ 14	−30 ≤ h ≤ 30	−26 ≤ h ≤ 26
	−18 ≤ k ≤ 17	−14 ≤ k ≤ 14	−16 ≤ k ≤ 16	−11 ≤ k ≤ 11	−10 ≤ k ≤ 10
	−30 ≤ l ≤ 31	−21 ≤ l ≤ 21	−18 ≤ l ≤ 18	−31 ≤ l ≤ 31	−26 ≤ l ≤ 25
Reflections collected	30989	29776	15763	23512	10378
Independent reflections	8406	7886	4356	5795	3558
	[R(int) = 0.1966]	[R(int) = 0.1376]	[R(int) = 0.1474]	[R(int) = 0.0337]	[R(int) = 0.0342]
Data	8406	7886	4356	5795	3558
Parameters	505	518	292	339	335
Goodness-of-fit on F^2	1.033	1.025	1.084	1.007	0.998
Final R indices [$I > 2\sigma(I)$]	$R1$ = 0.0701	$R1$ = 0.0572	$R1$ = 0.0703	$R1$ = 0.0417	$R1$ = 0.0380
	$wR2$ = 0.1258	$wR2$ = 0.1363	$wR2$ = 0.1843	$wR2$ = 0.1105	$wR2$ = 0.0980
R indices (all data)	$R1$ = 0.1624	$R1$ = 0.0792	$R1$ = 0.0916	$R1$ = 0.0586	$R1$ = 0.0526
	$wR2$ = 0.1609	$wR2$ = 0.1510	$wR2$ = 0.2266	$wR2$ = 0.1134	$wR2$ = 0.1036
Largest diff. peak/hole [e$^-$/Å^3]	0.581/−0.382	0.585/−0.667	1.076/−1.018	0.570/−0.662	0.587/−0.220

1575 (w), 1478 (vs), 1455 (vs), 1396 (w), 1378 (w), 1349 (w), 1330 (w), 1297 (w), 1271 (s), 1163(s), 1156 (m), 1120 (m), 1092 (s), 1038 (m), 1009 (s), 979 (w), 965 (w), 888 (s), 844 (w), 787 (vs), 757 (w), 738 (w), 726 (w), 656 (w), 641 (m), 576 (w), 524 (w), 495 (w), 474 (w).

$[Mn_2(L_4)_2(Cl)_2]\cdot CH_2Cl_2$ (4): Yield: 141.63 mg (0.14 mmol, 57%). $C_{40}H_{38}Cl_2Mn_2N_8O_6$ (907.57): calcd. C 52.93, H 4.22, N 12.35; found C 53.59, H 4.05, N 11.31. MS (MALDI): m/z = 870 [M$^+$ − HCl]. IR (KBr): $\tilde{\nu}$ = 3436 cm^{-1} (s, br), 3054 (w), 2955 (m), 2922 (m), 2675 (w), 2492 (w), 1974 (w), 1595 (s), 1575 (s), 1477 (s), 1437 (w), 1327 (w), 1287 (s), 1180 (m), 1127 (w), 1091 (s), 1051 (w), 1011 (m), 966 (w), 935 (m), 895 (w), 880 (w), 834 (m), 782 (m), 764 (m), 736 (w), 671 (m), 646 (m), 558 (w), 514 (w), 488 (w), 455 (w).

$[Mn_2(L_5)_2(Cl)_2]$ (5): Yield: 131.51 mg (0.16 mmol, 62%). $C_{40}H_{40}Cl_2MnN_6O_4$ (848): calcd. C 56.55, H 4.75, N 9.89; found C 56.23, H 4.89, N 9.24. MS (MALDI): m/z = 813 [M$^+$ − Cl]. IR (KBr): $\tilde{\nu}$ = 3429 cm^{-1} (s, br), 3055 (w), 2921 (m), 2849 (m), 1603 (s), 1571 (m), 1478 (vs), 1456 (m), 1441 (m), 1388 (w), 1346 (w), 1308 (m), 1273 (m), 1237 (m), 1154 (w), 1126 (w), 1079 (m), 1051 (m), 1014 (m), 1000 (m), 970 (w), 897 (w), 849 (m), 767 (m), 736 (m), 638 (w), 618 (w), 494 (w), 442 (w), 410 (w).

X-ray Crystallographic Study: Single-crystal X-ray studies of complexes **1**−**3** were performed with a Stoe IPDS diffractometer with graphite-monochromated Mo-K_α radiation (λ = 0.71073 Å) at 213 K; studies on compound **4** were done with a Bruker AXS SMART APEX with graphite-monochromated Mo-K_α radiation (λ = 0.71073 Å) at 100 K; studies on compound **5** were done with a Bruker AXS SMART 6000 with Cu-K_α radiation (λ = 1.54178 Å) at 100 K. All structures were solved with direct methods and refined by full-matrix least-squares procedures on F_o^2 values (SHELXTL-Plus-97[45,46]). Anisotropic displacement parameters were used to refine the positions of all non-hydrogen atoms. Hydrogen atoms were placed at calculated positions according to a riding model with group isotropic temperature factors. The residual value wR_2 in Table 5 is defined as $[w(F_o^2 - F_c^2)^2/w(F_o^2)^2]^{1/2}$. Selected distances and angles are listed in Tables 1−4. CCDC-205842 (**1**), -205843 (**2**), -205844 (**3**), -205845 (**4**), and -205846 (**5**) contain the supplementary crystallographic data for this paper. These data can be obtained free of charge at www.ccdc.cam.ac.uk/conts/retrieving.html [or from the Cambridge Crystallographic Data Centre, 12 Union Road, Cambridge CB2 1EZ, UK; Fax: (internat.) + 44-1223/336-033; E-mail: deposit@ccdc.cam.ac.uk].

Acknowledgments

Financial support by the DFG (Deutsche Forschungsgemeinschaft, SPP 1118) and the FCI (Fonds der Chemischen Industrie) is gratefully acknowledged.

[1] M. J. Maté, G. Murshudov, J. Bravo, W. R. Melik-Adamyan, P. C. Loewen, I. Fita, in *Handbook of Metalloproteins* (Eds.: A. Messerschmidt, R. Huber, T. Poulos, K. Wieghardt), John Wiley & Sons, New York **2001**, p. 468.
[2] Y. Kono, I. Fridovich, *J. Biol. Chem.* **1983**, *258*, 6015.
[3] W. F. Beyer Jr., I. Fridovich, *Biochem.* **1985**, *24*, 6460.
[4] V. V. Barynin, A. A. Vagin, W. R. Melik-Adamyan, A. I. Grebenko, S. V. Khangulov, A. N. Popov, M. E. Andrianova, B. K.

Vainshtein, *Dokl. Akad. Nauk SSSR* **1986**, *288*, 877; *Chem. Abstr.* **1986**, *105*, 74919q.
[5] V. V. Barynin, P. D. Hempstead, A. A. Vagin, S. V. Antonyuk, W. R. Melik-Adamyan, V. S. Lamzin, P. M. Harrison, P. Artymiuk, *J. Inorg. Biochem.* **1997**, *67*, 196.
[6] G. S. Allgood, J. J. Perry, *J. Bacteriol.* **1986**, *168*, 563.
[7] J. E. Penner-Hahn, in *Manganese Redox Enzymes* (Ed.: V. L. Pecoraro), VCH Publishers, Inc., New York, **1992**, p. 29.
[8] J. E. Penner-Hahn, *Struct. Bonding (Berlin, Ger.)* **1998**, *90*, 1.
[9] A. E. M. Boelrijk, G. C. Dismukes, *Inorg. Chem.* **2000**, *39*, 3020.
[10] P. Mathur, M. Crowder, G. C. Dismukes, *J. Am. Chem. Soc.* **1987**, *109*, 5227.
[11] P. J. Pessiki, S. V. Khangulov, D. M. Ho, G. C. Dismukes, *J. Am. Chem. Soc.* **1994**, *116*, 891.
[12] P. J. Pessiki, G. C. Dismukes, *J. Am. Chem. Soc.* **1994**, *116*, 898.
[13] A. Gelasco, S. Bensiek, V. L. Pecoraro, *Inorg. Chem.* **1998**, *37*, 3301.
[14] A. Gelasco, V. L. Pecoraro, *J. Am. Chem. Soc.* **1993**, *115*, 7928.
[15] A. Gelasco, M. L. Kirk, J. W. Kampf, V. L. Pecoraro, *Inorg. Chem.* **1997**, *36*, 1829.
[16] M. U. Triller, W.-Y. Hsieh, V. L. Pecoraro, A. Rompel, B. Krebs, *Inorg. Chem.* **2002**, *41*, 5544.
[17] S. Ito, S. Nishino, H. Itoh, S. Ohba, Y. Nishida, *Polyhedron* **1998**, *17*, 1637.
[18] S. Ito, M. Suzuki, T. Kobayashi, H. Itoh, A. Harada, S. Ohba, Y. Nishida, *J. Chem. Soc., Dalton Trans.* **1996**, 2579.
[19] H. Sugimoto, Y. Sasaki, *Chem. Lett.* **1997**, 541.
[20] A. Trösch, H. Vahrenkamp, *Eur. J. Inorg. Chem.* **1998**, 827.
[21] S. Yan, L. Que Jr., L. F. Taylor, O. P. Anderson, *J. Am. Chem. Soc.* **1988**, *110*, 5222.
[22] S. Yan, X. Pan, L. F. Taylor, J. H. Zhang, C. J. O'Connor, D. Britton, O. P. Anderson, L. Que Jr., *Inorg. Chim. Acta* **1996**, *243*, 1.
[23] H. Adams, N. A. Bailey, I. K. Campbell, D. E. Fenton, Q.-Y. He, *J. Chem. Soc., Dalton Trans.* **1996**, 2233.
[24] Y. Nishida, *Chem. Lett.* **1987**, *16*, 2151.
[25] U. Rajendran, R. Viswanathan, M. Palaniandavar, M. Lakshminarayanan, *J. Chem. Soc., Dalton Trans.* **1992**, 3563.
[26] R. Uma, R. Viswanathan, M. Palaniandavar, M. Lakshminarayanan, *J. Chem. Soc., Dalton Trans.* **1994**, 1219.
[27] M. Vaidyanathan, R. Viswanathan, M. Palaniandavar, T. Balasubramanian, P. Prabhaharan, T. P. Muthiah, *Inorg. Chem.* **1998**, *37*, 6418.
[28] R. Viswanathan, M. Palaniandavar, T. Balasubramanian, T. P. Muthiah, *Inorg. Chem.* **1998**, *37*, 2943.
[29] H.-R. Chang, S. K. Larsen, P. D. W. Boyd, C. G. Pierpont, D. N. Hendrickson, *J. Am. Chem. Soc.* **1988**, *110*, 4565.
[30] M. Marappan, V. Narayanan, M. Kandaswamy, *J. Chem. Soc., Dalton Trans.* **1998**, 3405.
[31] C. Hureau, E. Anxolabéhère-Mallart, M. Nierlich, F. Gonnet, E. Rivière, G. Blondin, *Eur. J. Inorg. Chem.* **2002**, 2710.
[32] D. P. Kessissoglou, W. H. Butler, V. L. Pecoraro, *Inorg. Chem.* **1987**, *26*, 495.
[33] J. Heinze, *Angew. Chem.* **1984**, *96*, 823; J. Heinze, *Angew. Chem. Int. Ed. Engl.* **1984**, *84*, 831.
[34] R. S. Nicholson, I. Shain, *Anal. Chem.* **1964**, *36*, 706.
[35] E. A. Lewis, J. R. Lindsay Smith, P. H. Walton, S. J. Archibald, S. P. Foxon, G. M. P. Giblin, *J. Chem. Soc., Dalton Trans.* **2001**, 1159.
[36] M. Shank, V. Barynin, G. C. Dismukes, *Biochemistry* **1994**, *33*, 15433.
[37] A. C. Rosenzweig, C. A. Frederick, S. J. Lippard, P. Nordlund, *Nature* **1993**, *366*, 537.
[38] E. J. Larson, V. L. Pecoraro, *J. Am. Chem. Soc.* **1991**, *113*, 7809.
[39] U. Bossek, M. Saher, T. Weyhermüller, K. J. Wieghardt, *J. Chem. Soc., Chem. Commun.* **1992**, 1780.
[40] C. Palopoli, B. Chansou, J.-P. Tuchagues, S. Signorella, *Inorg. Chem.* **2000**, *39*, 1458.
[41] J. F. Coetzee, in *Recommended Methods for Purification of Solvents*, Pergamon, Oxford, **1982**.
[42] R. Könecke, A. Comte, H. Jürgens, O. Kohls, H. Lam, T. Scheper, *Chem. Ing. Tech.* **1998**, *70*, 1611.
[43] *Handbook of Chemistry and Physics* (Ed.: R. C. Weast), 54th ed., CRC Press, Cleveland, **1973−1974**, B 116.
[44] Y. Nishida, H. Shimo, S. Kida, *J. Chem. Soc., Chem. Commun.* **1984**, 1611.
[45] G. M. Sheldrick, *SHELXS-97*, Universität Göttingen **1997**.
[46] G. M. Sheldrick, *SHELXL-97*, Universität Göttingen **1997**.

Received March 25, 2003
Early View Article
Published Online January 19, 2004

